INTERNATIONAL JOURNAL FOR NUMERICAL METHODS IN FLUIDS, VOL. 10, 373–400 (1990)

COMPARISON OF EXPERIMENTAL DATA WITH THE NUMERICAL SIMULATION OF PLANAR ENTRY FLOW: ROLE OF THE CONSTITUTIVE EQUATION

A. D. GOTSIS* AND D. G. BAIRD

Department of Chemical Engineering, Virginia Polytechnic Institute and State University, Blacksburg, VA 24060, U.S.A.

AND

J. N. REDDY

Engineering Science & Mechanics, Virginia Polytechnic Institute and State University, Blacksburg, VA 24060, U.S.A.

SUMMARY

The goal of this research was to determine whether there is any interaction between the type of constitutive equation used and the degree of mesh refinement, as well as how the type of constitutive equation might affect the convergence and quality of the solution, for a planar 4:1 contraction in the finite element method. Five constitutive equations were used in this work: the Phan-Thien–Tanner (PTT), Johnson–Segalman (JS), White–Metzner (WM), Leonov-like and upper convected Maxwell (UCM) models. A penalty Galerkin finite element technique was used to solve the system of non-linear differential equations. The constitutive equations were fitted to the steady shear viscosity and normal stress data for a polystyrene melt. In general it was found that the convergence limit based on the Deborah number *De* and the Weissenberg number *We* varied from model to model and from mesh to mesh. From a practical point of view it was observed that the wall shear stress in the downstream region should also be indicated at the point where convergence is lost, since this parameter reflects the throughput conditions. Because of the dependence of convergence on the combination of mesh size and constitutive equation, predictions of the computations were compared with birefringence data obtained for the same polystyrene melt flowing through a 4:1 planar contraction. Refinement in the mesh led to better agreement between the predictions using the PTT model and flow birefringence, but the oscillations became worse in the corner region as the mesh was further refined, eventually leading to the loss of convergence of the numerical algorithm. In comparing results using different models at the same wall shear stress conditions and on the same mesh, it was found that the PTT model gave less overshoot of the stresses at the re-entrant corner. Away from the corner there were very small differences between the quality of the solutions obtained using different models. All the models predicted solutions with oscillations. However, the values of the solutions oscillated around the experimental birefringence data, even when the numerical algorithm would not converge. Whereas the stresses are predicted to oscillate, the streamlines and velocity field remained smooth. Predictions for the existence of vortices as well as for the entrance pressure loss (ΔP_{ent}) varied from model to model. The UCM and WM models predicted negative values for ΔP_{ent}.

KEY WORDS Comparison Experimental Simulation Planar entry flow Viscoelastic Convergence

1. INTRODUCTION

The numerical simulation of flow of viscoelastic fluids into an abrupt contraction has received considerable attention in the past few years because it serves as a test problem for assessing the

* Present address: Chemistry & Chemical Engineering, Stevens Institute of Technology, Hoboken, NJ 07030, U.S.A.

0271–2091/90/040373–28$14.00

Received 19 May 1988
Revised 21 March 1989

difficulties associated with obtaining a numerically convergent and physically realistic solution.[1] Although significant progress has been made in resolving some of the difficulties that were initially encountered in the application of numerical methods (mainly finite difference and finite element methods), there still remains the problem of whether the numerical predictions are physically correct, even under conditions when the algorithm is convergent. The present paper is primarily concerned with the problem of whether it is possible to obtain physically realistic solutions, but it also addresses the problem of convergence. It includes the study of the combined effect of the mesh size and the constitutive equation on the convergence of the finite element method (FEM). It examines the quality of the numerical solutions by comparing them with experimental data obtained for similar flow conditions. Although the numerical method used here still suffers from the convergence problem, it serves to provide useful information about the role of the constitutive equation in generating physically realistic solutions.

Although the main thrust of the present article is not the loss of convergence of the numerical solutions, a brief review is necessary since the problem is so dominant. A detailed review on this topic up to 1983 can be found in the monograph by Crochet *et al.*[2] Furthermore, a brief review is necessary since it not only facilitates discussion of newer algorithms but also helps justify the work presented here. First we give a brief account of the initial ideas proposed as the cause of the loss of convergence and then discuss the latest methods for overcoming the breakdown of the numerical solution.

In general, it has been observed that as the elasticity of the flow increases, oscillations start to appear in the numerical solution, especially around singular points such as corners, boundary discontinuities or stagnation points, and the solution deteriorates quickly. At even higher elasticity levels the oscillations increase and the method ceases to converge. The limit of the Deborah (*De*) or the Weissenberg (*We*) number (these two dimensionless parameters are generally used as indicators of the elasticity level in the flow), above which no convergence could be achieved, depended on the type of the flow, the rheological model and the meshes that were used. Most disturbingly, the limits for convergence decreased as the mesh was refined.[3]

At first, the possible causes of the failure of convergence were divided into those related to the approximation error and those related to bifurcation or limit points.[4] By approximation error was meant the inability of the weighted residual method and the mesh to discretize the problem. There has been a lot of discussion in the literature about the existence of bifurcation or limit points in the solution of viscoelastic flows.[4-10] The existence of these singular points may be caused either by the full set of differential equations or by their discretized form.[5] However, the consensus now among authors on this subject is that when these points are found, they are the result of excessive approximation error.

In order to overcome these problems, several new approaches have been proposed. According to Debbaut *et al.*,[11] the excessive approximation error is associated with two aspects. One is the compatibility between the finite element approximations for velocity and stress. To overcome this problem, Marchal and Crochet[12] proposed a macro-element for velocity (biquadratic approximations) subdivided into $n \times n$ elements for stress (bilinear approximations). The other aspect is related to the change in type of the system equations from elliptic to hyperbolic, as the elasticity level becomes high.[13] More specifically, DuPret *et al.*[14] showed that numerical inaccuracies caused by singularities or boundary layers can lead to such an artificial change of type of the equations. To overcome this, Marchal and Crochet used a streamline upwinding method developed by Brooks and Hughes.[15] The accuracy of these methods has not been evaluated at this time.

King *et al.*[16] used another approach to address the problem of change of type of the system of equations. On the basis of ideas by Renardy,[17] they proposed a formulation of the momentum

equation that makes the elliptic character of this equation explicit. No special elements seemed to be needed when using this approach.

In spite of the success of the two methods described above and that of special methods described by Beris *et al.*[18] to obtain convergent solutions at higher levels of elasticity, there are still problems with each approach. For the case of additive diffusion, according to King *et al.*[16] smooth solutions can be computed which do not approximate well the fine structure of stress and velocity fields in boundary layers and near singularities. In the case of the explicitly elliptic momentum equation the method is limited at present to whether one can find the appropriate form for a given constitutive equation. In the case of spectral methods[18] it is not possible to use the method for problems with re-entrant corners. Hence, although new algorithms have been developed recently, none is completely satisfactory at this point.

In this paper we address those aspects that must be considered no matter what method is used. First there is the role played by the constitutive equation in obtaining results which are physically realistic. In particular *We* and *De* can be greater than 1·0 for a given constitutive equation but the overall stress be quite low. Furthermore, some constitutive equations seem to be easier to obtain smooth solutions for than others. Secondly, in this paper we provide direct evidence for the loss of the numerical solution arising at the re-entrant corners in planar entry flow. Finally, we evaluate whether the use of linear approximations for stress and velocity in the penalty/Galerkin finite element method provides reasonable solutions which agree well with experimental data.

2. RHEOLOGICAL EQUATIONS OF STATE

The rheological equation of state that is used to describe the material in the simulated flow will influence both the quality of the solution and its convergence behaviour. In the present report, five different rheological models were used to study their effect on convergence and for comparison of the numerical results. These models were the Phan-Thien–Tanner (PTT), the Johnson–Segalman (JS) the Leonov-like, the White–Metzner (WM) and the upper convected Maxwell (UCM) models and were chosen because of the variety in their predictions in simple shear and extensional flows. A summary of these predictions is given in the following. The interested reader should look at References 19–24 for details on the derivation of the models.

2.1. Leonov-like model

The model proposed by Leonov[19,20] was derived from irreversible thermodynamic principles, is an extension of rubber elasticity to viscoelastic media and can be considered as a non-linear form of the generalized Maxwell model with n relaxation times and a viscous retardation term. The retardation term may also include strain hardening. A simplified form of the Leonov model with one relaxation time and no retardation term is the Leonov-like model[21]

$$\boldsymbol{\tau} + \lambda \boldsymbol{\tau}_{(1)} + \frac{\lambda}{2\eta_0} \boldsymbol{\tau} \cdot \boldsymbol{\tau} = \eta_0 \dot{\boldsymbol{\gamma}}, \tag{1}$$

where $\boldsymbol{\tau}_{(1)}$ denotes the upper convected time derivative of $\boldsymbol{\tau}$.[25] In simple shear flow this model is the same as the original Leonov model and its predictions are

$$\eta = \frac{2\eta_0}{1 + \sqrt{(1 + 4\lambda^2 \dot{\gamma}^2)}}, \tag{2}$$

$$\Psi_1 = \sqrt{2}\, \frac{\eta_0 \sqrt{(1 + 4\lambda^2 \dot{\gamma}^2)} - 1}{\lambda \sqrt{(1 + 4\lambda^2 \dot{\gamma}^2)} + 1}. \tag{3}$$

The elongational viscosity $\bar{\eta}$ predicted by this model is equal to $3\eta_0$ at low extension rates and increases asymptotically to $6\eta_0$ at high extension rates.

From the set of equations (2) and (3), the relaxation parameters for a specific fluid can be evaluated by fitting either the viscosity (η) or the primary normal stress difference (N_1). By evaluating the parameters with one set of data and predicting the other, it has been shown that the model fits well the viscometric data.[22]

2.2. *Phan-Thien–Tanner model*

While the model proposed by Leonov was derived from continuum mechanics and thermodynamics arguments, the Phan-Thien–Tanner model was derived from molecular considerations and was based on the ideas of non-affine network theories.[23,24] The model has the form of the upper convected generalized Maxwell model with extra non-linear terms in the stress:

$$\tau = \sum \tau^i, \tag{4}$$

$$\lambda_i \tau^i_{(1)} + \exp\left(\frac{\lambda_i \varepsilon}{\eta_i} \mathrm{tr}(\tau^i)\right)\tau^i + \frac{\lambda_i \xi}{2}(\dot{\gamma}\cdot\tau^i + \tau^i\cdot\gamma) = \eta_i \dot{\gamma}. \tag{5}$$

In addition to the relaxation times and viscosities, this model employs parameters ξ, which represents the non-affineness of the network, and ε, which represents the rate of destruction of the temporary network junctions. A finite value of ε results in a maximum in the change of the extensional viscosity with extension rate, and ξ causes the viscosity to shear-thin rapidly to the degree that a maximum appears in the shear stress versus shear rate curve. A retardation term has been added to correct this, the value of which has to be greater than 1/9 the zero shear rate viscosity.

The PTT model with one relaxation mode and such a retardation term is expressed as follows:

$$\tau = \tau^1 + \tau^2, \tag{6}$$

$$\lambda \tau^1_{(1)} + \exp\left(\frac{\lambda \varepsilon}{\eta} \mathrm{tr}(\tau^1)\right)\tau^1 + \frac{\lambda \xi}{2}(\dot{\gamma}\cdot\tau^1 + \tau^1\cdot\dot{\gamma}) = \eta_1 \dot{\gamma}, \tag{7}$$

$$\tau^2 = \eta_2 \dot{\gamma}, \tag{8}$$

with τ^1 the viscoelastic stress and τ^2 a purely viscous stress. The predictions of this model in simple shear flow are

$$\eta = \frac{\eta_1}{[1 + \xi(2 - \xi)\lambda^2\dot{\gamma}^2]} + \eta_2, \tag{9}$$

$$N_1 = \frac{2\eta_1 \lambda \dot{\gamma}^2}{[1 + \xi(2 - \xi)\lambda^2\dot{\gamma}^2]}, \tag{10}$$

$$N_2 = -\frac{\xi}{2} N_1. \tag{11}$$

The relaxation parameters of the PTT model can be evaluated in the same way as for the Leonov model. The parameter ξ is usually evaluated from a horizontal shift between the dynamic (η') and the simple shear viscosity curves according to the following equation:[23]

$$\eta'(x) = \eta\left(\frac{x}{\sqrt{[\xi(2 - \xi)]}}\right). \tag{12}$$

The predictions of the model in simple shear flow are insensitive to the value of ε. This parameter has to be evaluated from elongational viscosity data.[24]

2.3. Other models

Besides the PTT and the Leonov-like models, the upper convected Maxwell, the White–Metzner and the Johnson–Segalman models were also used. The first two models are widely used in flow calculations because of their simplicity. They were used in this work in the following form:[25]

$$\tau + \lambda \tau_{(1)} = \eta \dot{\gamma}. \tag{13}$$

In this relation the viscosity and the relaxation time coefficients (η and λ) of the UCM model are constants, while for the WM model they are empirical functions of the second invariant of the rate of deformation tensor.

The Johnson–Segalman model is similar to the PTT model but does not contain the term with the parameter ε. As a result, it predicts an unbounded extensional viscosity at high extension rates. Its predictions in simple shear flow are very close to the predictions of the PTT model.

2.4. Parameters of the models

The principal polymeric materials for which all the calculations were done was a polystyrene melt (PS) of weight-average molecular weight of 255 000 (trade name STYRON 678, made by Dow Chemical Co.). Viscometric data for this material at 190 °C are given in Reference 26 and were used to evaluate the parameters of all models. The zero shear viscosity and the relaxation times in the PTT and the Leonov-like models were evaluated from the viscosity curve with the help of equations (2), (3), (9) and (10). The relaxation time and the viscosity coefficient of the UCM and the WM models were evaluated from both N_1 and η data. Non-linear least squares fit techniques were used to evaluate the parameters.

Table I. Values for the coefficients of the rheological models to fit the simple shear behaviour of STYRON 678 at 190 °C

Model	Value of the coefficient
Phan-Thien–Tanner	$\eta_1 = 9660$ Pa s
or	$\eta_2 = 1288$ Pa s
Johnson–Segalman	$\lambda = 0{\cdot}5$ s
	$\xi = 0{\cdot}2$
	$\varepsilon = 0{\cdot}015$ (PTT only)
White–Metzner	$\eta_1 = \eta_0[1 + (m\dot{\gamma})^2]^{(n-1)/2}$
	$\eta_2 = 0$
	$\eta_0 = 11100$ Pa s
	$m = 4{\cdot}0$ s
	$n = 0{\cdot}67$
	$\lambda = 0{\cdot}43504 - 0{\cdot}45297 \log_{10}\dot{\gamma} + 0{\cdot}1388 (\log_{10}\dot{\gamma})^2$
Upper convected	$\eta_1 = 11100$ Pa s
Maxwell	$\lambda = 0{\cdot}6$ s
Leonov-like	$\eta_1 = 10400$ Pa s
	$\eta_2 = 624$ Pa s
	$\lambda = 0{\cdot}6$ s

The data over the shear rates measured did not show any indication of an infinite shear rate plateau viscosity. For the retardation viscosity of the PTT model, the value of $\eta_1/\eta_2 = 7{\cdot}5$ was chosen here, with the understanding that the model will not describe the experimental data at high shear rates (above $60\,s^{-1}$). Even though a retardation term was not necessary for the Leonov-like model, a value of 6% of the zero shear rate viscosity was used for the infinite shear rate plateau, because it was found that the presence of such a term stabilized the method without affecting the results considerably. The parameter ξ in the PTT model was evaluated by equation (12). At the time of this work there were no elongational data available at high extension rates and hence ε of the PTT model could not be evaluated. A value of 0·015 was used, which is thought to give a good estimate for polymeric melts.[24] The parameters of all the models are shown in Table I. The fit of the various models to the viscometric data is shown in Figures 1–3.

3. THE FINITE ELEMENT MODEL

The equations that are solved in the problem of isothermal flow of incompressible viscoelastic fluids are the equations of conservation of momentum, conservation of mass and the constitutive equation. When inertia terms and gravity are neglected, these equations in Cartesian component form become*

$$\tau_{ij,\,j} - P_{,i} = 0, \tag{14}$$

$$u_{i,\,j} = 0, \tag{15}$$

$$h_k(\tau_{ij}, \dot{\gamma}_{ij}, u_i) = 0, \tag{16}$$

where h_k is a differential operator that can have the form of equations (1), (6)–(8) or (13), τ_{ij} is the extra stress tensor, $\dot{\gamma}_{ij}$ is the rate of deformation tensor and u_i is the velocity vector.

The penalty/Galerkin finite element method was used in the present work to discretize the equations above. In this method the equation of continuity is considered as a constraint on the equation of momentum and the pressure P is approximated by using a large positive number γ_p (the penalty parameter) such that

$$P = -\gamma_p(u_{i,i}). \tag{17}$$

The incompressibility constraint is imposed by substituting this approximation into the momentum equation. The velocity and stress profiles are then obtained as the solution of the system of the modified momentum equation and the constitutive equation. The convergence of the solution to the incompressible solution is affected by the choice of the penalty parameter. In principle, the higher the value of γ_p the more incompressible the solution becomes. It has been found that a value of γ_p of the order of 10^6 times the viscosity will give accurate results for Newtonian flows.[27] The penalty method, however, has been found to require a reduced order for the integration of the penalty terms in order to obtain non-trivial solutions.[28] The integration of the penalty term was carried over one Gauss point in the linear elements and over four in the quadratic elements, while for the other terms the integrations were carried over four and nine points, respectively.

The Galerkin weak form of the equation of motion is obtained after the substitution into equation (14) of τ from equations (6)–(8), the incorporation of the penalty term (equation (18)) and the application of the divergence theorem. The weak form of the continuity equation is not

* The Einstein notation is used here in which the repeated indices in the same term imply summation.

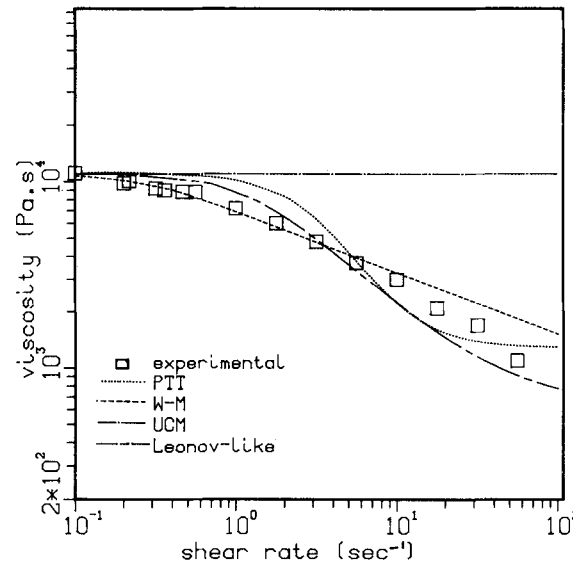

Figure 1. Viscosity versus shear rate for STYRON 678 at 190 °C. The lines represent predictions of the rheological models

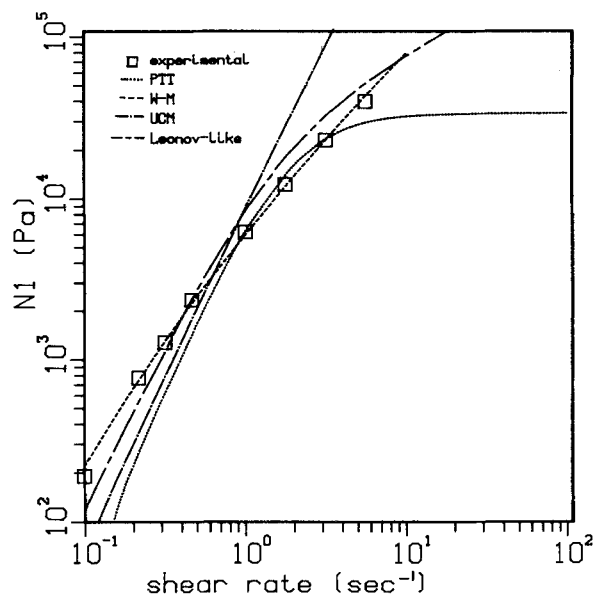

Figure 2. Primary normal stress difference of STYRON 678 at 190 °C

needed because of the use of the penalty method. Integration by parts is not performed for the weak forms of the constitutive equations because only first-order derivatives are present. The solution of the non-linear system of equations generated in the FEM was accomplished by means of a Picard iteration. In this technique the nodal values of the velocity and the stress from the previous iteration are used to evaluate the non-linear terms of the current iteration. The linearized

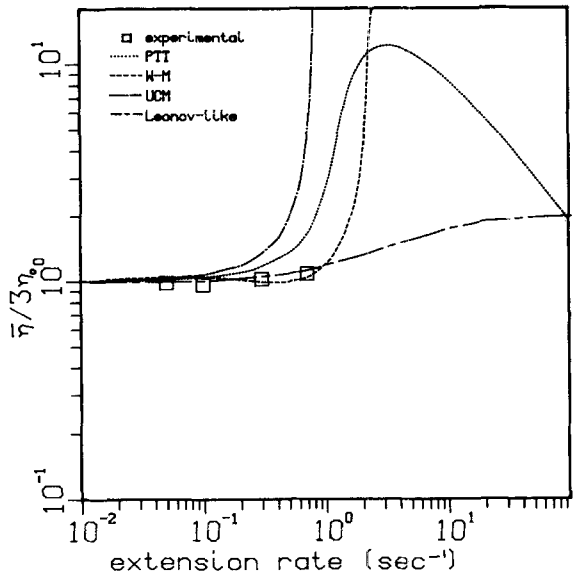

Figure 3. Extensional viscosity of STYRON 678 at 190 °C

system can thus be solved. The Newtonian solution was used as the initial guess and the iterations ended when the change between successive iterations became less than a specified tolerance. Details of the form of the final equations that were inserted in the computer algorithm to solve the discretized problem can be found in Reference 26.

There is still some discussion in the literature on viscoelastic flows as to the degree of the shape functions which should be used for the velocities, the stresses and the pressure. It has been shown that the shape functions used for the pressure in the mixed formulation should be an order less than the velocities.[2] The use of the penalty method, however, eliminates the pressure as a variable. The choice for the shape functions for the velocities and the stresses may thus include linear polynomials. In the present work, either bilinear or biquadratic (serendipity) isoparametric elements were used with the same order interpolation polynomials for the velocity and the stress in each case.

The boundary conditions that were used for the entry flow were the specification of the velocity profile at the entrance and exit of the flow domain, no slip at the wall and zero normal component of the velocity along the centreline. The stresses were also specified at the entry plane. The lengths of two upstream (2H) and four downstream (4*h*) channel heights from the contraction were used for the imposition of the fully developed velocity profile. There are several reports on the subject of how far away from the corner these boundary planes should be set. It has been found that insufficient distances may not only result in incorrect solutions but may also introduce instability into the numerical method.[8] Detailed reports on this effect are given in References 8 and 29. In the case of the present study, the distances that were used were selected on the basis of experimental observations of how far from the corner the flow seemed undisturbed.[30] This choice was also justified *a posteriori* from the results of the calculations, where the changes due to the contraction were dissipated at distances less than half the upstream and downstream lengths of the meshes (see Figures 9 and 11).

The velocity profiles that were imposed at the entrance and exit of the domain were calculated as one-dimensional problems of pressure-driven flow between parallel plates for each constitutive

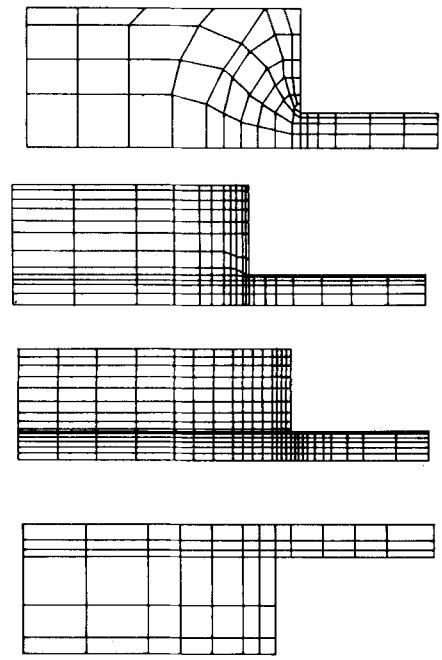

Figure 4. Meshes used in the computations

equation. This gave considerably different profiles for flows under similar stress levels and flow rates because of the different shear-thinning behaviour predicted by the constitutive equations.

Four meshes were used in the calculations. Three of them had linear elements (MESH1, MESH2 and MESH3) and the fourth (MESH4) had biquadratic serendipity elements. The number of nodes was 97 for MESH1, 204 for MESH2, 332 for MESH3 and 208 for MESH4. The four meshes are shown in Figure 4.

4. RESULTS AND DISCUSSION

4.1. Comparison of convergence limits

The limits in the convergence of the solution at high elasticity levels that were found in the present calculations are shown in Table II. This table gives the limits of the elasticity levels, the shear stress on the wall on the downstream channel (τ_w) and the flow rate (Q) that could be achieved before the divergence of the solution occurred. These last two parameters were used for comparisons in this work, since predictions for the elasticity level varied from model to model. as will be explained in the following, and because they are usually the critical parameters in actual extrusion processes.

From Table II it may be seen that the limits of convergence differ widely from one model to the next. But before examining these differences, the problem of the basis of the comparison has to be mentioned. In most reports where comparisons between models are given, the basis for these comparisons was the level of elasticity of the flow as given by the Deborah (De) or the Weissenberg number (We). The main advantage for this choice is the fact that these two numbers show the extent of the difference between the viscoelastic and the Newtonian nature of the flow.

Table II. Limits of convergence for all the combinations of models and meshes

Mesh	Model	τ_{12w}[a] (kPa)	Q/W[b] ($mm^2\ s^{-1}$)	Dc[c]	We[d]
1	PTT	34	17·54	11·41	1·55
	JS	33	16·44	10·95	1·59
	WM	43·5	14·05	1·42	1·42
	Leonov-like	24	8·21	7·49	1·79
	UCM	32	3·29	1·84	1·84
2	PTT	27	9·32	7·98	1·90
	JS	27	9·32	7·98	1·90
	WM	34	9·93	1·23	1·23
	Leonov-like	22	6·37	5·85	1·68
	UCM	24	2·32	1·30	1·30
3	PTT	24	5·71	6·17	2·08
	JS	24	5·71	6·17	2·08
	WM	20	4·42	0·92	0·92
	Leonov-like	17·5	3·49	3·01	1·32
	UCM	19	1·84	1·03	1·03
4 (quadratic)	PTT	25	6·90	6·82	2·03
	JS	25	6·90	6·82	2·03
	WM	27	8·56	1·17	1·17
	Leonov-like	18	3·59	3·11	2·33
	UCM	20	1·94	1·08	1·08

[a] τ_{12w}, wall shear stress at a point far downstream from the contraction.
[b] Q/W, flow rate per unit width.
[c] $De = \lambda\dot{\gamma}_w$.
[d] $We = (N_1/2\tau_{12})_w$.

Another reason for this choice is that *De* or *We* may in some cases be used directly in the equations as dimensionless parameters and no specific choices for viscosity, relaxation time coefficient or absolute stress levels have to be made. However, this choice is not sufficient for comparing different rheological models in real situations since the same elasticity level will result in predictions of different flow and stress fields. The reason for this uncertainty is that each model will only describe approximately the properties of the materials of interest here, as for example the shear-thinning viscosity. In flow between parallel plates, then, for a model that predicts shear-thinning viscosity, the stress levels will be lower than those predicted by the UCM model for the same flow rate and the same Deborah number.

There is another reason why an elasticity parameter should not be used as an absolute criterion for the comparison between rheological models. In Figure 5 are shown the predictions of *We* ($= N_1/2\tau_{12}$) in simple shear flow for the models that were used in this work but with their coefficients evaluated to fit the same polystyrene melt. It can be seen from this figure that the predictions of the models for the same material and the same simple flow are significantly different, especially at high shear rates. Further, the experimental data in the same figure indicate that *We* may actually level off at high shear rates. No model can describe this behaviour, except perhaps the White–Metzner model (at low shear rates), whose parameters were determined from experimental data using both the shear stress and the primary normal stress difference. On the contrary, *We* for the PTT and the JS models shows a maximum and then decreases with increasing shear rate, whereas the Leonov-like model climbs to much higher values of *We*. The slope of the curve that corresponds to the UCM model is approximately double the slope of the

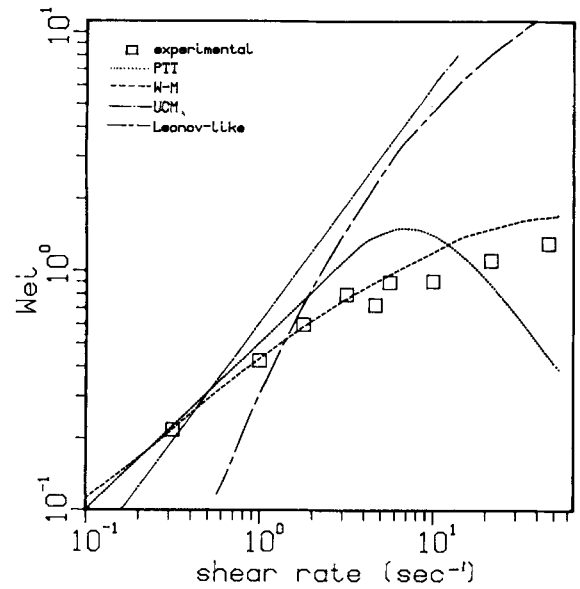

Figure 5. Weissenberg number in simple shear flow as a function of shear rate for STYRON 678 at 190 °C

experimental data. In any case, if the experimental values of *We* tend to level off at a value of 1·5–2·0, there will be a discrepancy between experimental and theoretical results when comparisons are made with numerical results that may show values of $We = 6$ or even 9. In other words, obtaining solutions at a so-called high value of *De* for a given constitutive equation may be meaningless when making comparisons between their predictions and experimental data.

The need for another basis of comparison is then obvious. The relative importance of the elasticity number remains, since there is always a limiting value for convergence, but additional criteria have to be used. Because the same material and the same geometry are considered in all calculations here, it is suggested in Table II that the values of the stress at some characteristic point may also be used as the basis for such comparisons. The flow rate is another important quantity that can be used, especially for industrial applications, and it is also included in Table II.

In terms of the maximum wall shear stress it can be seen that the White–Metzner model shows the best results. The PTT and the JS models come next, showing approximately equal limits, and the Leonov-like model is found to give the lowest limits. When the comparison is done in terms of the flow rates, the picture in somewhat different. For MESH1, the PTT and the JS models will exhibit higher limits than the WM model. For the other two meshes the latter will handle higher flow rates than the two former ones. The difference between the limits of the stress and the flow rates can be explained by the differences that these models predict in the shear-thinning viscosity (Figure 1) and this underlines the difficulty of comparing results obtained by different rheological models.

Comparing the results between the different meshes, it may be seen that all the limits decrease with the refinement of the mesh. When the number of nodes doubles, as in going from MESH1 to MESH2, the decrease is around 20%–25%. An increase of 50% in the number of the nodes from MESH2 to MESH3 results in an additional 20% decrease of the limits for convergence. The lowest decrease of the limit of convergence with mesh refinement is shown by the Leonov-like model, but this model shows limits consistently lower than the other models. The maximum effect

of the mesh is found for the WM model, which decreases to such a degree that in the finest mesh it shows lower limits than the PTT model.

Higher limits of convergence were achieved using a mesh with linear elements (MESH2) than by using a mesh with quadratic elements and the same number of nodes (MESH4), something somewhat unexpected. Yeh *et al.*[6] and Debbaut and Crochet[8] have reported that a higher order of interpolation polynomials would be more likely to show higher limits. It is possible that the apparent contradiction between these reports and the present results is due to differences between the mixed FEM formulation (velocities, stresses and the pressure as field variables) that the above authors used and the penalty/FEM formulation that was used here.

The limits of convergence for the PTT model in this work are at the same levels as the results reported earlier.[8] It should be noted that the definition of *De* for the PTT model in these two articles is different from the one used here. If the Deborah number is defined as $De = \sqrt{[\xi(2 - \xi)]}\lambda\dot{\gamma}$ (as in Reference 8), the values of the limits in Table II for this model should become 6·8, 4·8 and 2·64 for MESH1, MESH2 and MESH3 respectively. The limits of convergence for the Leonov-like model compare well with those reported by Keunings and Crochet,[31] who used meshes with a similar number of nodes but quadratic elements, and are lower than the ones reported by Isayev and Upadhyay,[32] who used the full model. The dependence of the convergence on the specific mesh, however, makes the quantitative comparison between the results of this work and those reported in the literature very difficult. Comparisons, therefore, are more meaningful between theoretical results and experimental data obtained for the same material under the same flow conditions and between numerical solutions obtained with the same mesh. Since for most viscoelastic models there is no analytical solution with which to compare the numerical results, the only available method to examine the accuracy of the solution and its improvement (or worsening) with the refinement of the mesh or the use of a different rheological equation is to compare it with experimental results. In the following subsection the accuracy of the numerical results will be examined by comparing the stresses and the streamlines from the FEM solutions with stresses and streamlines measured experimentally for the same flow conditions. The experimental results come from flow birefringence measurements reported in Reference 30.

4.2. Stress field comparison

In a flow birefringence experiment, the isochromatic fringes of the stress field are obtained using circularly polarized light and the stress optic law. For a 2D flow field the fringe order is given as follows:[33]

$$\bar{N} = \frac{WC}{\lambda'}\sqrt{[(\tau_{11} - \tau_{22})^2 + 4\tau_{12}^2]}, \tag{18}$$

where λ' is the wavelength of the laser beam, W is the thickness of the fluid through which the light travels and C is the stress optic coefficient. In this equation the Cartesian co-ordinates are defined so that '1' is the direction of the flow, '2' is the direction perpendicular to the flow surfaces and '3' is the third co-ordinate, along which the laser beam is directed.

The experimentally measured fringes are compared directly with the contours of $\bar{N}$ (evaluated from equation (18)) using the calculated values of the stresses at each point. This comparison can be seen in Figure 6 for a 4:1 contraction flow and a wall shear stress o 16 kPa evaluated in the downstream region. The numerical results shown in this figure come from calculations using the four different meshes and the PTT model. Figure 7 shows the same contour plots calculated using MESH3 and three different rheological models for the same downstream wall shear stress level of

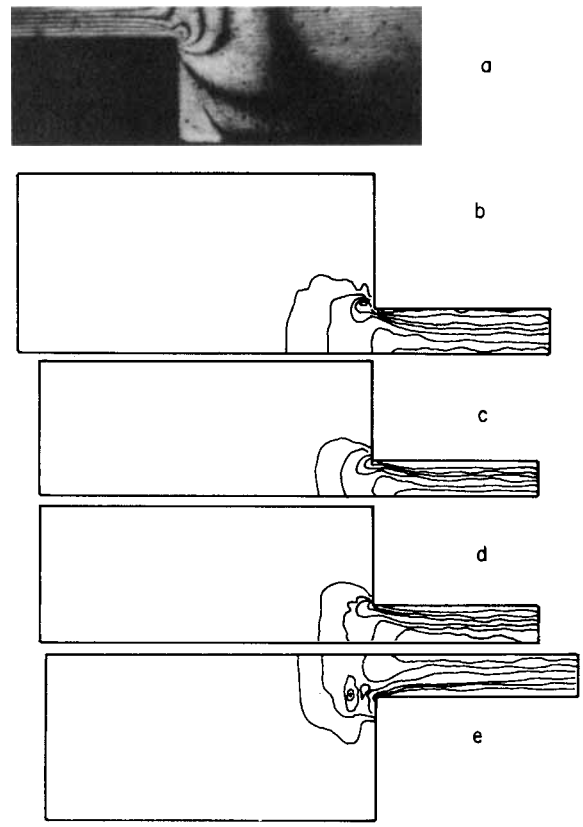

Figure 6. Experimental and calculated contours of fringe order in 4:1 contraction flow using the PTT model: (a) experimental; (b) MESH1; (c) MESH2; (d) MESH3; (e) MESH4. $\tau_w = 16$ kPa

16 kPa. From these figures it can be seen that all four meshes give an acceptable overall picture for the isochromatic fringes at these stress levels. Also, there is no distinguishable qualitative difference between the solutions obtained from the several models, something that is probably due to the low stress levels. The numerical results of all the meshes show a maximum in $\bar{N}$ at a point upstream from the corner. The presence in the numerical results of other peaks near the corner is probably due to oscillations of the calculated stresses, as will be described below.

In order to quantify the comparisons between the results of the numerical simulation and the experimental data, plots were made of the birefringence results taken or calculated along vertical and horizontal lines around the re-entrant corner. The lines along which $\bar{N}$ was plotted are shown in Figure 8. The values of the fringe order along the lines AB and CD around the contraction can be seen in Figure 9 as calculated for the four meshes by the PTT model and compared to the experimental data. The values of $\bar{N}$ along the lines EF and GH are shown in Figure 10. It should be noted for these figures that $\bar{N}$ takes on a high value for $x > 0$ (downstream) because of the fast downstream flow. Upstream ($x < 0$) the stresses along AO are lower, not only because of the greater height of the channel but also because this line lies relatively closer to the centreline. The experimental results reach the value of the downstream channel asymptotically, while the numerical results show an overshoot near the corner (around $x = 0{\cdot}2h$ in Figure 9).

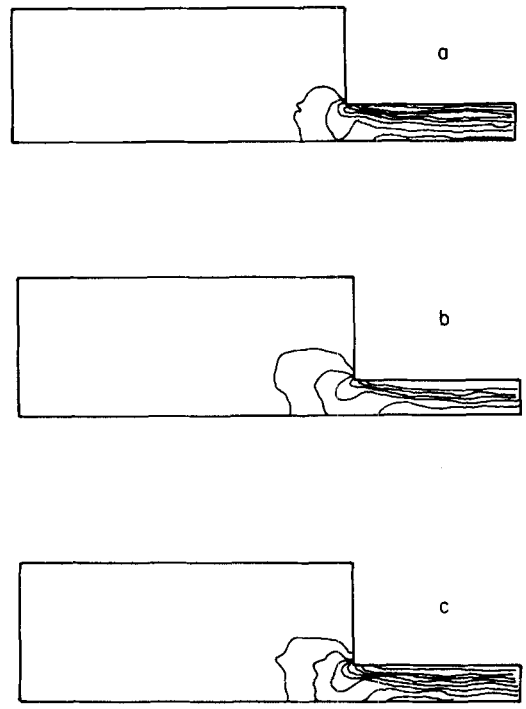

Figure 7. Calculated contours of fringe order in 4:1 contraction flow using MESH3: (a) UCM; (b) WM; (c) Leonov-like model. $\tau_w = 16$ kPa

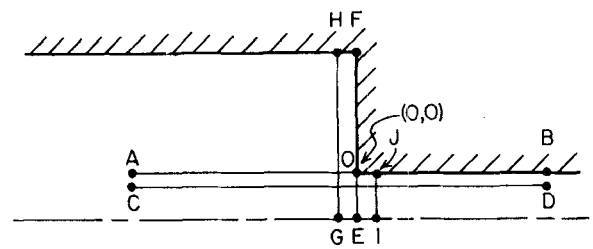

Figure 8. Lines in the flow domain along which the values of the fringe order are plotted in Figures 9–12

From Figure 9 it can be seen that oscillations are found around the re-entrant corner in this flow. The lowest apparent oscillations in the upstream channel are found for the coarsest mesh (MESH1). The oscillations in the results based on MESH3 are more pronounced near the entry plane and extend up to $x = -3h$ upstream and $x = 1{\cdot}5h$ downstream, a distance which is common for all the meshes. MESH2 leads to oscillations, the magnitude of which is intermediate between those of the other two meshes with linear elements. MESH4 also shows high oscillations. All calculated values, however, oscillate around the experimental points.

Along the line $y = -0{\cdot}2h$ the oscillations are reduced to some degree (Figure 9(b)). Here all the meshes show a local maximum at a point around $0{\cdot}2h$ upstream, then a minimum at $x = 0$ and finally $\bar{N}$ rises asymptotically to its unperturbed value in the exit region of the die. This local maximum is probably an oscillation because the experimental data only show a small shoulder

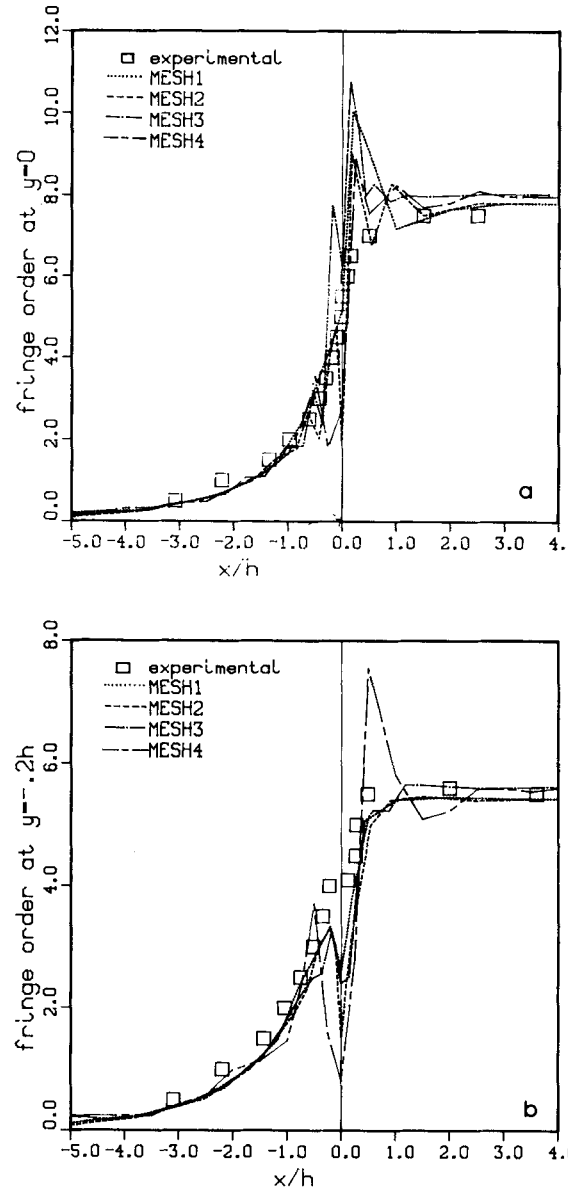

Figure 9. (a) Fringe order along line $y = 0$. (b) Fringe order along line $y = -0{\cdot}2h$. PTT model and different meshes. $\tau_w = 16$ kPa

around $x = 0$ and then continue to rise. No overshoot is shown by either the experimental or the numerical results in the downstream channel, except in the results obtained using MESH4.

Following y on the entrance plane from the top blind corner towards the centreline (from right to left in Figure 10(a)), it can be seen that the values of $\bar{N}$ increase rapidly near the re-entrant corner, showing a maximum near $y = 0$. The fringe order then decreases towards the centreline ($y = -h$), but it does not become zero there because there is a strong elongational flow field along this line around the entrance plane, since the fluid has to accelerate to enter the narrower channel.

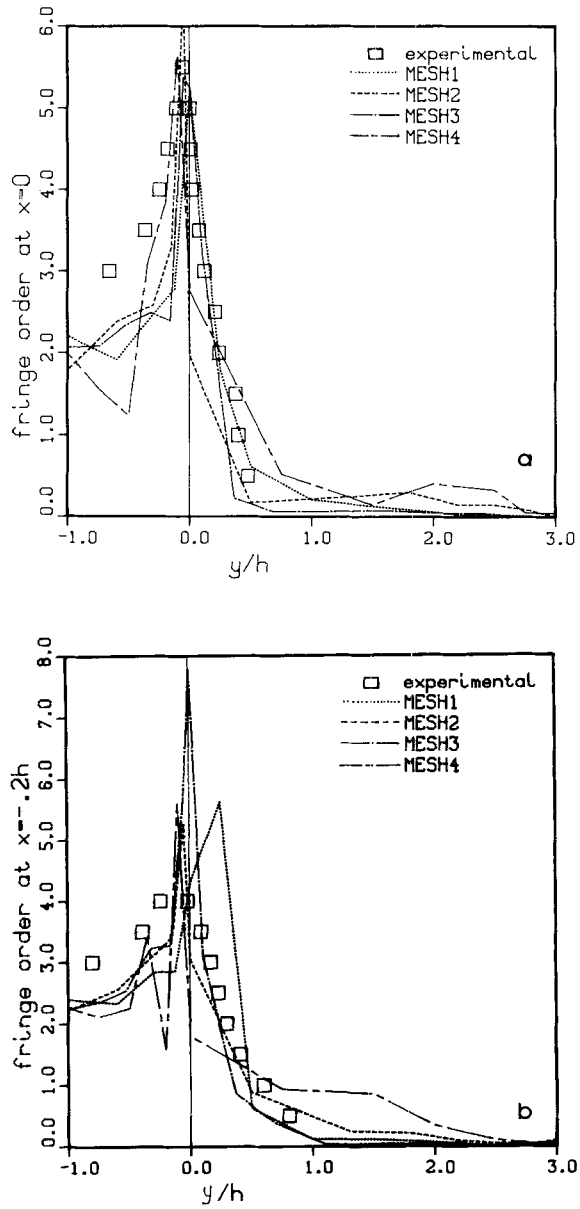

Figure 10. (a) Fringe order along line $x = 0$. (b) Fringe order along line $x = -0{\cdot}2h$. PTT model and different meshes. $\tau_w = 16$ kPa

The values of N predicted by all the meshes are approximately the same at the centreline. The experimental data also show the abrupt increase near the corner and a maximum around $y = -0{\cdot}1h$, in good agreement with the results of MESH2 and MESH3. The agreement at $y < 0$, however, is not so good, since the data show higher values than those obtained by means of numerical solutions using the PTT model.

The value of $\bar{N}$ along y at the line $x = -0{\cdot}2h$, somewhat upstream from the contraction, can be seen in Figure 10(b). Strangely enough, the oscillations of the numerical solution seem to be worse

here, even though this line lies further from the singularity at the corner. This is probably due to the fact that this line falls on the maxima and minima of the oscillations observed in Figure 9. The highest oscillations are shown when MESH4 is used. Clearly the results of MESH1 and MESH4 are unacceptable. Even though the increase of $\bar{N}$ near the corner for $y > 0$ agrees well with the results of MESH2 and MESH3, the overshoot at $y = 0$ in the numerical results is higher than the experimental data.

Summarizing the differences between the results obtained using different meshes but the same model (PTT), it may be seen that for this flow the coarsest mesh will give the lowest oscillations. The agreement with the experimental data is, however, the poorest for this mesh. The finer meshes with linear elements show worse oscillations and higher peaks, but their results agree better with the experimental data at points away from the corner. At the corner itself the overshoots in the numerical solution are much higher than the experimental ones. The quadratic mesh gives worse results than MESH2, which has the same number of nodes. It seems that the numerical method that was developed here works better with linear than with quadratic elements. This is contradictory to what was reported in Reference 8, where higher-degree polynomials improved the solution. Again a possible explanation for this contradiction may be related to the penalty formulation that was used here instead of the mixed method that was used in Reference 8. The results obtained here should be compared with results obtained for the same flow conditions and using the mixed formulation in order to clear these questions.

For the comprison of the results of different rheological equations, similar plots to those in Figures 9 and 10 were made. Figures 11 and 12 show the fringe order calculated using the four models and MESH3. It can be seen there that the results of all the models show similar oscillations. The overall agreement between the numerical results and the experimental data is good except in the neighbourhood of the corner ($x = 0$ in Figure 11 and $y = 0$ in Figure 12). In that area all the models show oscillations and high overshoots which are absent from the data. The highest overshoots are shown by the UCM model and the best agreement in the exit channel is shown by the White–Metzner model. Oscillations are also found along the line $y = 0{\cdot}2h$, indicating that high stress gradients extend to some distance from the corner for all the models. The results of all the models fall very close to each other in these graphs.

The picture of the stresses in the extensional field at the centreline around the entrance can be seen better from a plot of the normal stress difference along this line. Since the shear stress is zero there, $\tau_{xx} - \tau_{yy}$ can be calculated directly from the birefringence data (using equation (19)). These results together with the results of the computations are shown in Figure 13. The normal stress difference starts rising at a distance around $x = 5h$ upstream form the contraction, shows a maximum at $x = -0{\cdot}4h$ and approaches zero again at $x = +3h$. Even though the behaviour of the models is qualitatively correct as compared to the experimental data, only the WM and the Leonov-like models show good quantitative agreement with the data. It should be noted here that the extension rates that occur along the centreline at these flow conditions are low enough, so that $\bar{\eta} = 3\eta_0$ for all the models. The differences in the extensional viscosity predictions of the models that were described earlier cannot be responsible for the disagreement between the different curves in Figure 13.

In summary, the comparison between the experimental and numerical results shows that a reasonable stress field for the flow into a contraction can be calculated by the FEM/penalty method using any of the five rheological models. Oscillations are found around the re-entrant corner, indicating that there may exist a numerical singularity in the stresses at this point. A coarse mesh (like MESH1) will smooth these oscillations to some degree. The agreement of the results of MESH1 with the experimental data is poor, however, making this mesh unacceptable. MESH2 and MESH3 give results in good agreement with the experimental data except in the

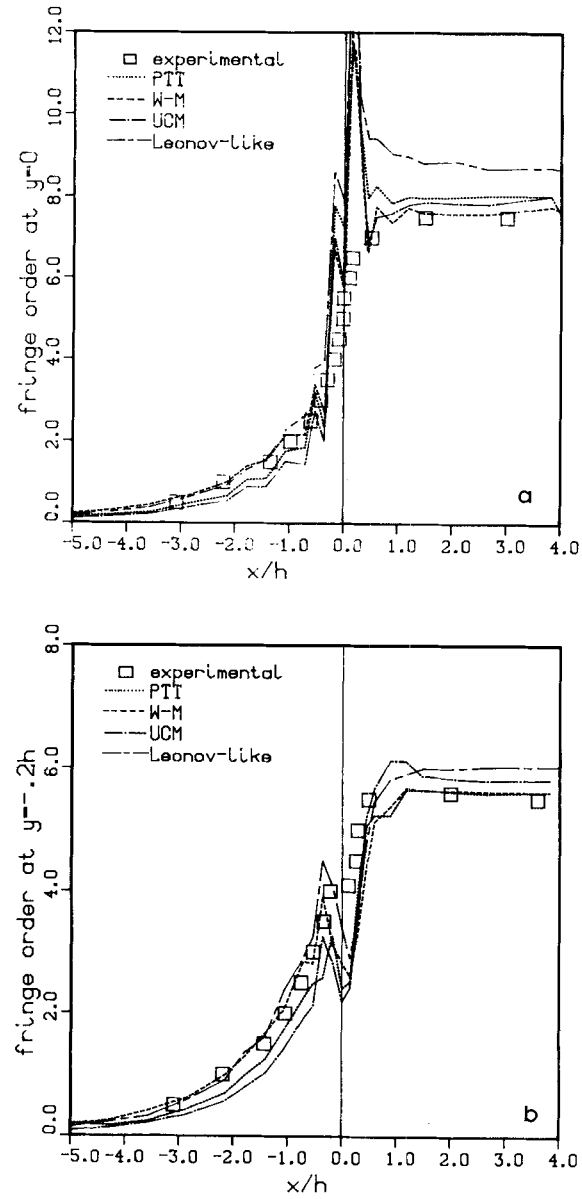

Figure 11. (a) Fringe order along line $y = 0$. (b) Fringe order along line $y = -0{\cdot}2h$. MESH3 and different models. $\tau_w = 16$ kPa

very vicinity of the re-entrant corner. High peak values of the stresses are found a little upstream from the corner, a reason for the extension of the oscillations at a longer distance upstream than downstream. The comparison of the rheological models shows that the WM and the Leonov-like models will give the best predictions over the range of conditions reported here. These two models will also show the best results in the extensional field along the centreline. The PTT and the UCM models show lower values for the stresses there, but their results elsewhere are very close to the

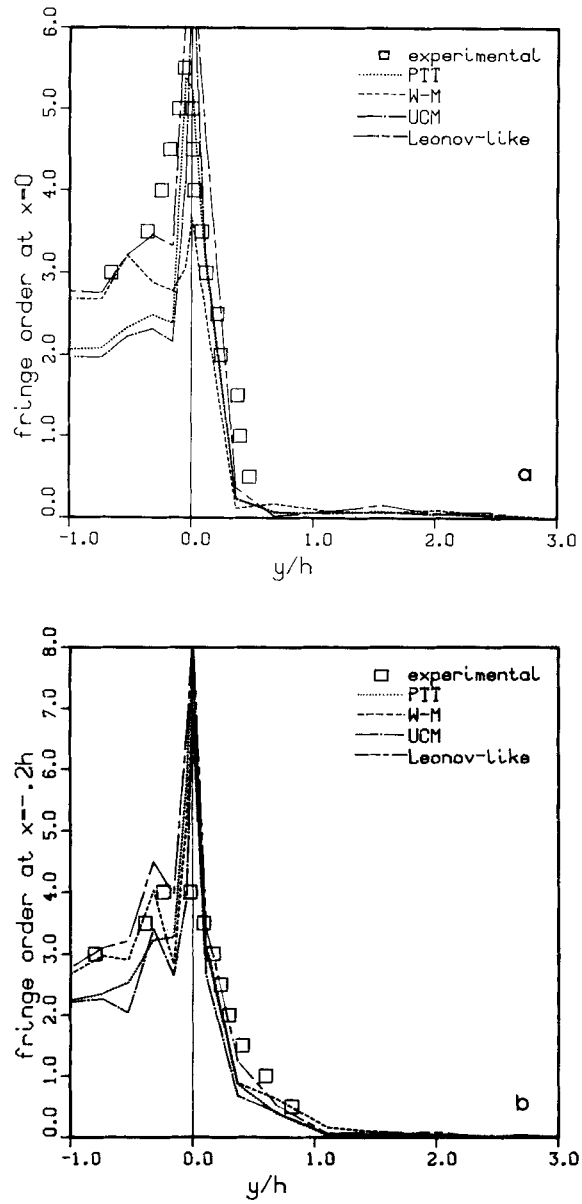

Figure 12. (a) Fringe order along line $x = 0$. (b) Fringe order along line $x = -0{\cdot}2h$. MESH3 and different models. $\tau_w = 16$ kPa

results of the other two models. Some of the disagreement, however, may be due to the inability of the models to fit the rheological data exactly.

4.3. Entrance pressure loss

The extra pressure drop caused by the contraction is a characteristic of the flow of viscoelastic fluids and accounts for the extra energy that is needed to accelerate and deform the elastic fluid

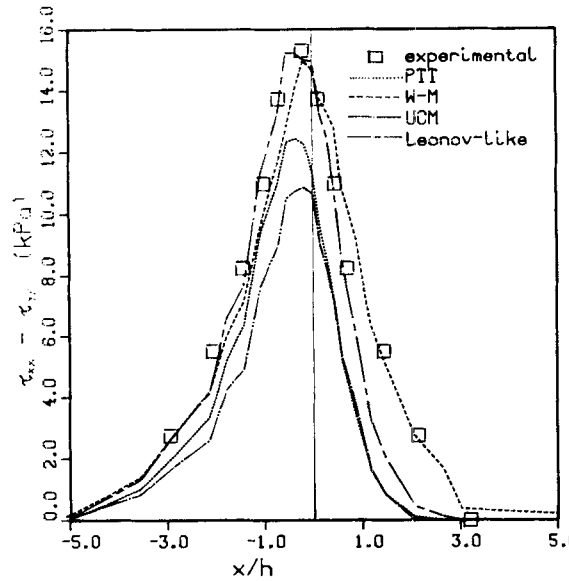

Figure 13. Normal stress difference ($\tau_{xx} - \tau_{yy}$) along the centreline using MESH3. $\tau_w = 16$ kPa

elements as they flow into the exit channel. The entrance pressure loss has been found experimentally to be positive and it may be associated with the extensional viscosity of a polymeric fluid. It has also been proposed as an important quantity with which to compare numerically determined values. In order to define the entrance pressure loss in the present work, two points were chosen on the wall in the undisturbed regions, one upstream (A) and one downstream (B). The entrance pressure loss is the difference between the total pressure drop between A and B minus the sum of the pressure drops that would occur in isolated entry and exit channels between A or B, respectively, and the entrance plane.

The isotropic pressure was a secondary variable in the penalty formulation and was calculated from the velocity field in the postprocessing step. It was found in the present study that the predictions for the entrance pressure loss were very little affected by the mesh refinement. The predictions using various rheological models were very different, however, as can be seen in Figure 14, where the entrance pressure loss (ΔP_{ent}) is plotted against the wall shear stress (τ_w). It can be seen in this figure that ΔP_{ent} increases monotonically with the wall shear stress for the PTT and the Leonov-like models. The UCM and the WM models, however, show a maximum in ΔP_{ent}. As τ_w increases further, the entrance pressure loss decreases and eventually becomes negative. Negative values for ΔP_{ent} were also found by Keunings and Crochet for the Olroyd-B and the UCM models.[31] The results in that report compared qualitatively well with the present results. Because of these negative values, the PTT and the Leonov-like models seem to be better than the UCM and the WM models for calculations of entrance pressure losses. It is not known at this time what leads to the predictions of negative values of ΔP_{ent} for some models, but it is certainly not an acceptable result. This also suggests that we must consider carefully whether it is appropriate to use those models which give negative values for ΔP_{ent} in further computations.

4.4. Streamlines

The formation of the vortex in the blind corner upstream of the contraction is examined in this subsection by studying the picture of the streamlines. It was demonstrated in Reference 1 that

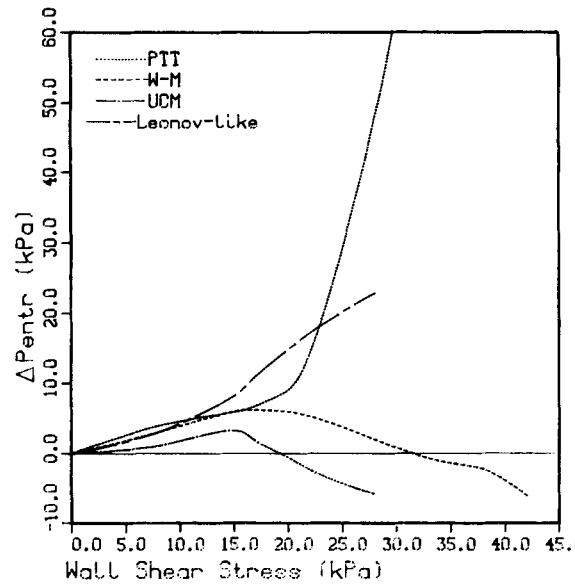

Figure 14. Entrance pressure loss in planar 4:1 contraction

some polymeric fluids will show strong vortices in planar entry flow while others will show at most very weak vortices of constant size under the same flow conditions. The material (PS at 190 °C) that was used as a test fluid in this work was found experimentally to exhibit only small vortices[34] which did not grow with *We* under flow conditions similar to the ones that were simulated here. The comparisons of the observed streamlines with the normalized results of the several meshes and the PTT model, as well as the results of the other models using MESH3, are shown in Figures 15 and 16.

The streamlines calculated using the PTT model and for all four meshes agree very well with each other away from the entrance plane, as should be expected. All the meshes show that the streamline closest to the wall starts moving away from the wall of the upstream channel at a distance of around $x = -4h$ from the entrance plane, leaving a triangular region around the blind corner. For MESH1 this region is slightly smaller than the other meshes and the angle with which the streamline approaches the re-entrant corner is steeper. The values of streamlines at this triangular region are too low to be plotted and well within the approximation error. For MESH2 and MESH3, however, the weak recirculating vortex in that region has a (normalized) intensity of $-0{\cdot}001$, which is quite low and may also be within the approximation error. The validity of this vortex, however, is supported by the fact that it starts appearing when the mesh is refined (instead of disappearing with finer meshes as was the case in Reference 35, and its position is the same and its intensity is consistent among runs under different flow rates (it decreases with decreasing flow rate). The velocity vectors also show a very slow recirculating motion in the same area[26] for the finer mesh.

Debbaut and Crochet[8] and Keunings and Crochet[31] also found such a vortex for the PTT model under similar elasticity levels. The vortex intensity that was reported in these articles was higher than the one calculated here, perhaps because the normalization of the streamlines was done differently or because the parameters of the model (PTT) that was used were different. Because of its very small intensity, however, the existence of this vortex may be of rather small rheological importance. In another paper[36] we discuss the possible influence of the parameter ε of this model on the existence and intensity of the calculated vortex.

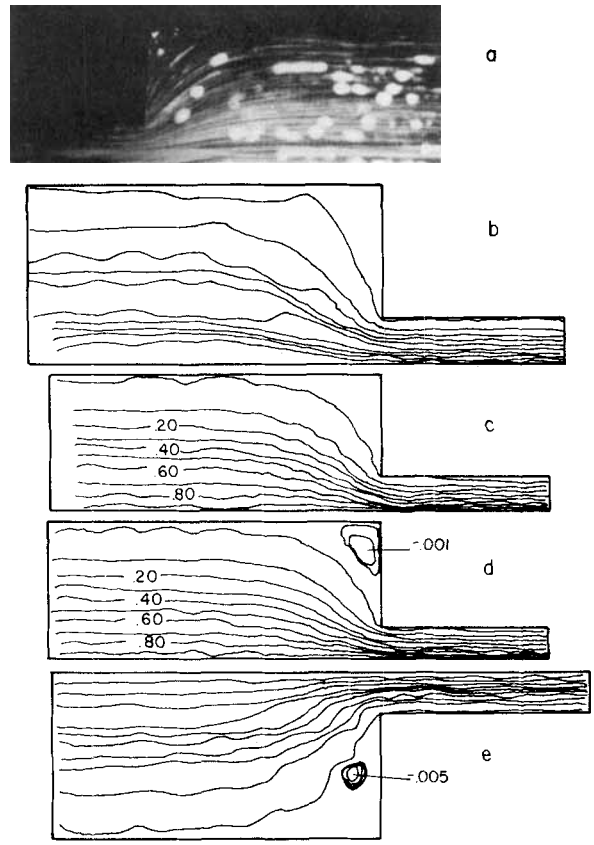

Figure 15. Calculated streamlines using the PTT model and different meshes. (a) experimental; (b) MESH1; (c) MESH2; (d) MESH3; (e) MESH4. $\tau_w = 16$ kPa

Under the same stress levels as above, all the rheological models showed a vortex (Figure 16). It should be noted, however, that the flow rates for each model in Figure 16 are different because of the differences in the predictions of shear-thinning viscosity. The fact that the vortex predicted by the WM model is much stronger and larger than the other models is probably due to the higher flow rate that this model shows under the same shear stress level. Another possible reason for this stronger vortex may be the fact that the ratio $\bar{\eta}/\eta_0$ as predicted by this model is higher than the ones predicted by the other models under these conditions (Figure 3). Vortices were found to be formed more easily in experiments with fluids that show higher values for this ratio.[30] The weakest vortex is shown by the UCM model, something which may be due to the lower flow rate that this model predicts for a given value of shear stress. For this model it was found in References 35 and 37 that such a vortex was only a numerical artefact.

4.5. Elongational rates in the flow field

The acceleration field around the contraction was examined in a previous subsection by observing the normal stress difference along the centreline. This line, however, is not the only area in the flow field with a high extensional flow component. There is another area near the re-entrant corner where, in addition to shear flow, the fluid elements also undergo extensional deformation.

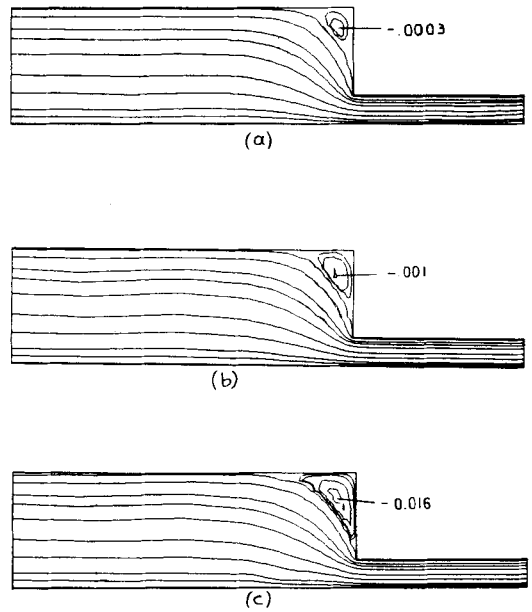

Figure 16. Streamlines in 4:1 contraction flow using MESH3 and different models: (a) UCM; (b) Leonov-like; (c) WM. $\tau_w = 16$ kPa

In order to define a measure of the extensional deformation in a two-dimensional field with both extension and shear deformation and to be consistent with the quantity that is used in uniaxial extension measurements, the extension rate ($\dot{\varepsilon}$) in this work is defined as

$$\dot{\varepsilon} = \sqrt{\left\{\frac{2}{3}\left[\left(\frac{\partial u_x}{\partial x}\right)^2 + \left(\frac{\partial u_y}{\partial y}\right)^2\right]\right\}}. \tag{19}$$

In uniaxial extension this measure will reduce to the same $\dot{\varepsilon}$ that was used in defining the Trouton viscosity in Figure 3.

The second area with high extension rates can be seen in the contour plot of $\dot{\varepsilon}$ (Figure 17). This area lies around a line starting at the re-entrant corner and extending at a 45° angle towards the wall upstream. The point with the highest value of $\dot{\varepsilon}$ in the flow domain is located on that line, a little away from the corner, in the same area where the maximum in the birefringence also occurs (see Figure 9). It seems that the birefringence in this area comes more from the contribution of the extensional stresses than the shear stresses. Further, the angle that this line makes to the horizontal may be related to the 'natural entry angle', the angle at which the viscoelastic fluid enters the downstream channel.[30] Some researchers use this angle as a measure of the size of vortex that may exist at the blind corner upstream. If the vortex calculated from the streamlines in this work is compared to this angle, it can be seen that the natural entry angle should be around 70° rather than 45°. It is possible that these two angles above are related but do not coincide.

In the numerical solution of the flow into the contraction, the values of the maximum extension rate ($\dot{\varepsilon}_{max}$) were found near the re-entrant corner. These values for each model and mesh at their limits of convergence are shown in Table III, together with the values of the critical extension rate in uniaxial extension ($\dot{\varepsilon}_{crit}$), above which the models predict an infinite value for $\bar{\eta}$ in uniaxial extensional flow. As is expected, the values of $\dot{\varepsilon}_{max}$ decrease with the refinement of the mesh. However, in the coarsest mesh the value of $\dot{\varepsilon}_{max}$ is higher than $\dot{\varepsilon}_{crit}$. This is reversed in finer meshes.

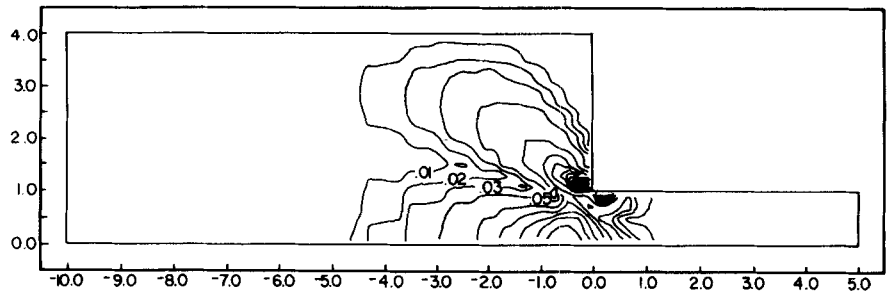

Figure 17. Contours of extensional strain rate (calculated using equation (19)) in planar 4:1 contraction, predicted by the PTT model using MESH3. $\tau_w = 16$ kPa

Table III. Critical extension rates for the rheological models and maximum extension rates (see equation (19)) found in the calculations

Model	Mesh	$\dot{\varepsilon}_{max}$ (s^{-1})	$\dot{\varepsilon}_{crit}$ (s^{-1})	Position of maximum
PTT	1	2·87	—	−0·1, 0·01
	2	2·54		−0·16, 0·0
	3	2·07		−0·26, 0·05
JS	1	2·78	1·25	−0·1, 0·01
	2	2·57		−0·16, 0·0
	3	2·09		−0·26, 0·05
Leonov-like	1	2·43	—	−0·1, 0·01
	2	1·83		−0·16, 0·0
	3	1·14		−0·26, 0·05
WM	1	3·18	2·4	−0·1, 0·01
	2	1·88		−0·16, 0·0
	3	1·20		−0·26, 0·05
UCM	1	1·44	0·83	−0·1, 0·01
	2	0·79		−0·16, 0·0
	3	0·59		−0·26, 0·05

It is believed here that the coarse discretization of MESH1 actually smooths out the unbounded peak of the stresses that should result from an extension rate higher than $\dot{\varepsilon}_{crit}$. This unbounded value of the extensional viscosity is not the only cause of the lack of convergence of the numerical solutions, as can be seen from the existence of limits even in models that do not show much unbounded values. This was also reported by Keunings,[38] who showed that the limit may go to zero for an infinitely fine mesh even for the Leonov-like model, a model which shows an extensional viscosity that grows gently with extension rate, approaching $6\eta_0$ asymptotically.

4.6. Behaviour of the solution at the limit of convergence

Much was said about the problem of convergence in the numerical calculations for the viscoelastic flows and its possible relation to the existence of singular points at the corners. The oscillations that were found around the corner and their increase with the mesh refinement give indications of such a spatial singularity. Lipscomb *et al.*[39] gave evidence for the presence of a

singularity for a second-order fluid and a UCM model. Following the presence of oscillations in the results of the present calculations with the PTT and the Leonov-like models, as well as reports by Keunings and Crochet,[31] it is believed that such singularities are not avoided by these two models either.

Figure 18 shows the evolution of the oscillations in $\bar{N}$ along the line $y = 0$ for values of wall shear stress of 20, 24 and 26 kPa, given by the PTT model using MESH3. At a wall shear stress of 24 kPa the convergence was marginal. At 26 kPa the method did not converge and the results correspond to the iteration with the least error. The values of the birefringence in this figure are normalized for the comparison by division by the values of $\bar{N}$ at the downstream wall for each curve. It can be seen that as the wall stress level increases, the oscillations around the re-entrant corner also increase in magnitude and extend further upstream and downstream. However, there is no qualitative difference in the solution for a wall shear stress of 26 kPa from the solutions at lower stress levels. It seems that the accumulation of the error at that point is just too large for the method to converge.

Because of the lack of a sudden change in the values of the stresses upon the transition from convergence to divergence of the solution, it is interesting to see whether the results obtained at 26 kPa wall shear stress agree with the experimental data (Figure 19). The comparison near the corner is impossible because of the high oscillations of the numerical results and also because the resolution of the experimental technique is reduced at high stress levels, where there are many fringes in the same area. The results a little away from the corner, however, are close to the experimental data. Following this and considering the parametric family of solutions with the stress at the wall (or the elasticity *De*) as the parameter, it seems that the limit of convergence does not occur at some singular value of this parameter, such as a limit or a bifurcation point. That is, such points that have been found elsewhere may be only numerical artefacts, something that has already been suggested in Reference 8. Rather, the divergence occurs because of accumulation of error above the level that the method can handle. This error may be connected with the possible

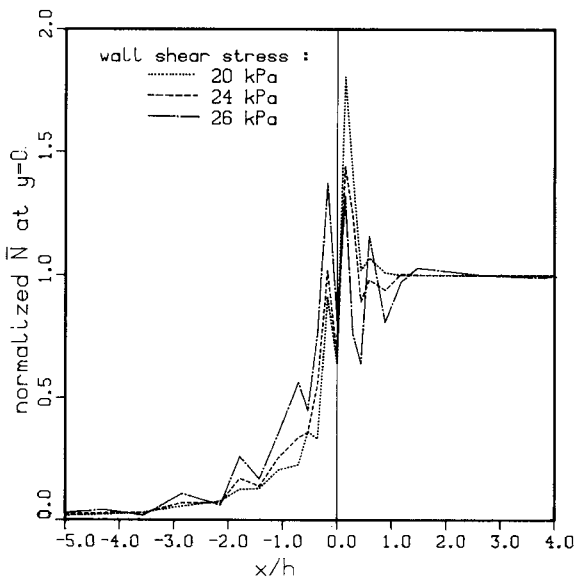

Figure 18. Change of the oscillations of the stresses around the corner as the stress level increases and the limit of convergence is passed. MESH3 and PTT were used. The limit for this combination of model and mesh was 24 kPa

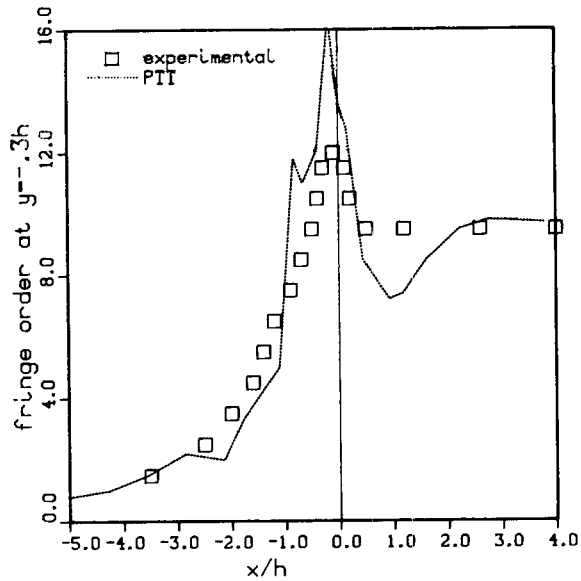

Figure 19. Stress around the corner for a solution that did not converge. PTT and MESH3

existence of a spatial singularity of the stresses at the corner. This problem, therefore, will not be avoided in finer meshes. The results in the present paper seem to confirm the conclusions by Lipscomb *et al.*[39] that the effect of such a singularity will be enhanced if the size of the elements around the corner is reduced and the convergence will deteriorate. Of course there is also the possibility of the change of type of the differential equations in the same region, as was mentioned earlier.[40, 41]

5. CONCLUSIONS

It is well known that one cannot escape the convergence problem merely by the choice of the viscoelastic constitutive equation. At some critical value of fluid elasticity the numerical solution will fail regardless of which constitutive equation is selected. However, reports of convergence limits at Deborah numbers as high as 10·0, for example, can be misleading and, furthermore, they can be functions of the constitutive equation used in the computations. For example, for a mesh containing 256 elements and 290 nodes, the critical values of *De* for convergence are 7·98 for the PTT model but only 1·23 for the WM model. On the other hand, the wall shear stress values in the downstream region of the die are 27 and 34 kPa for the respective models. Hence we recommend that when specifying the limits of convergence, some other parameters be specified, such as wall shear stress, volumetric flow rate or average velocity. Otherwise the numerical solutions may be of little value at what appears to be an extraordinarily high level of fluid elasticity.

Another point that is to be made is that there seems to be a range of mesh refinements over which reasonable solutions can be obtained, as confirmed by the comparison with flow birefringence data. Unfortunately there are no guidelines or rules for selecting an appropriate mesh refinement. On the other hand, there is a wide range of convergence limits obtained by using various rheological models. The UCM model was found to give the lowest limits, while the WM and the PTT models show the highest limits for convergence, when the comparison was based on the wall shear stress or the volumetric flow rate. However, no significant differences were found

between the results of the various models when the calculations were done for wall shear stress levels at which all the models would converge, except in the results of the entrance pressure loss, where the predictions of negative values for ΔP_{ent} by the UCM and the WM models may render them unacceptable to use.

Finally, the loss of convergence may be attributed to the inability of the Galerkin finite element method to handle the stress gradients at the re-entrant corners. As the stress levels increase because of increasing flow rate, the stresses at the corner are predicted to become quite large in a relatively small area and begin to oscillate. The approximation error then grows, causing the numerical solution not to converge. Even though the stresses are oscillating, they oscillate around the measured values. When the solution fails to converge, the oscillations grow in amplitude but still occur about the measured values of stress. These results add further support that the convergence problems may be due to approximation errors.

ACKNOWLEDGEMENTS

This work was supported by grants from the Center for Innovative Technology/Institute for Materials Science and Engineering (Grant No. MAT-87-018) and the Petroleum Research Fund (Grant No. PRE 16119-AC7-C).

APPENDIX: LIST OF SYMBOLS

$\dot{\gamma}, \dot{\gamma}_{ij}$	rate of deformation tensor
$\dot{\gamma}_w$	wall shear rate downstream from the contraction
τ, τ_{ij}	extra stress tensor
τ_w	wall stress downstream from the contraction
$\dot{\gamma}$	second invariant of rate of deformation tensor
$\dot{\varepsilon}$	extensional strain rate
De	Deborah number, $\lambda\dot{\gamma}_w$
We	Weissenberg number, $(\tau_{xx} - \tau_{yy})/2\tau_{xy}$
h	half-height of downstream channel
H	half-height of upstream channel
η	viscosity
η_0	zero-shear-rate viscosity
η_i	viscosity coefficients
$\bar{\eta}$	extensional viscosity
η'	dynamic viscosity
λ, λ_i	relaxation times
N_1	primary normal stress difference
Ψ_1	primary normal stress difference coefficient
$\bar{N}$	fringe order
λ'	wavelength of laser beam in birefringence measurements
C	stress optic coefficient
W	width of die
ξ	non-affinity parameter for the PTT model
ε	extensional parameter in the PTT model
γ_p	penalty parameter
ΔP_{ent}	entrance pressure loss
Q	volumetric flow rate

REFERENCES

1. S. A. White, A. D. Gotsis and D. G. Baird, *J. Non-Newtonian Fluid Mech.*, **24,** 121 (1987).
2. M. J. Crochet, A. R. Davies and K. Walters, *Numerical Simulation of Non-Newtonian Flows, Rheology Series, Vol. 1*, Elsevier, 1984.
3. M. J. Crochet, *J. Non-Newtonian Fluid Mech.*, **20,** 1 (1986).
4. M. A. Mendelson, R. A. Brown and R. C. Armstrong, *J. Non-Newtonian Fluid Mech.*, **10,** 31 (1982).
5. A. R. Davies, *J. Non-Newtonian Fluid Mech.*, **16,** 195 (1984).
6. P. W. Yeh, M. E. Kim, R. C. Armstrong and R. A. Brown, *J. Non-Newtonian Fluid Mech.*, **16,** 173 (1984).
7. R. Keunings, *J. Comput. Phys.*, **62,** 199 (1986).
8. B. Debbaut and M. J. Crochet, *J. Non-Netwonian Fluid Mech.*, **20,** 173 (1986).
9. S. L. Josse, K.-C. Lee and B. A. Finlayson, *J. Non-Newtonian Fluid Mech.*, **20,** 257 (1986).
10. J. V. Lawler, S. J. Muller, R. A. Brown and R. C. Armstrong, *J. Non-Newtonian Fluid Mech.*, **20,** 51 (1986).
11. B. Debbaut, J. M. Marchal and M. J. Crochet, *J. Non-Newtonian Fluid Mech.*, **29,** 119 (1988).
12. J. M. Marchal and M. J. Crochet, *J. Non-Newtonian Fluid Mech.*, **26,** 77 (1987).
13. D. D. Joseph, M. Renardy and J. C. Saut, *Arch. Rat. Mech. Anal.*, **27,** 213 (1985).
14. F. DuPret, J. M. Marchal and M. C. Crochet, *J. Non-Newtonian Fluid Mech.*, **18,** 173 (1985).
15. A. N. Brooks and T. J. R. Hughes, *Comput. Math. Appl. Mech. Eng.*, **32,** 199 (1982).
16. R. C. King, M. R. Appelian, R. C. Armstrong and R. A. Brown, *J. Non-Newtonian Fluid Mech.*, **29,** 147 (1988).
17. M. Renardy, 'Existence of slow steady flows of viscoelastic fluids with differential constitutive equations', *Z. Angew. Math. Mech.*, **62**(9), 449 (1985).
18. A. Beris, R. C. Armstrong and R. A. Brown, *J. Non-Newtonian Fluid Mech.*, **22,** 129 (1987).
19. A. I. Leonov, *Rheol. Acta*, **15,** 85 (1976).
20. A. I. Leonov and M. N. Prokounin, *Rheol. Acta*, **19,** 393 (1980).
21. R. G. Larson, *Rheol. Acta*, **22,** 435 (1983).
22. R. K. Upadhyay, *Ph.D. Dissertation*, Cornell University, 1982.
23. N. Phan-Thien and R. I. Tanner, *J. Non-Newtonian Fluid Mech.*, **2,** 313 (1977).
24. N. Phan-Thien and R. I. Tanner, *J. Rheol.*, **22**(3), 259 (1978).
25. R. B. Bird, R. C. Armstrong and O. Hassager, *Dynamics of Polymeric Liquids, Vol. 1*, Wiley, 1977.
26. A. D. Gotsis, *Ph.D. Dissertation*, Virginia Polytechnic Institute and State University, 1986.
27. S. Nakazawa, J. F. T. Pittman and O. C. Zienkievicz, 'Numerical solution of flow and heat transfer in polymer melts', in *Finite Elements in Fluids, Vol. 4*, Wiley, 1982, p. 251.
28. J. N. Reddy, *Int. j. numer. methods fluids*, **2,** 151 (1982).
29. J. S. Vrentas and M. C. Vrentas, *J. Non-Newtonian Fluid Mech.*, **19,** 1 (1985).
30. S. A. White, *Ph.D. Dissertation*, Virginia Polytechnic Institute and State University, 1987.
31. R. Keunings and M. J. Crochet, *J. Non-Newtonian Fluid Mech.*, **14,** 279 (1984).
32. A. I. Isayev and R. K. Upadhyay, *Rheol. Acta*, **25,** 80 (1986).
33. D. Pike, *Ph.D. Dissertation*, Virginia Polytechnic Institute and State University, 1985.
34. S. A. White and D. G. Baird, *J. Non-Newtonian Fluid Mech.*, **29,** 245 (1988).
35. R. I. Tanner, 'On the stability of computations in processing rheology', in *Proc. IX Int. Congr. on Rheology*, Mexico, 1984.
36. S. A. White, D. G. Baird and A. D. Gotsis, *J. Non-Newtonian Fluid Mech.*, **30,** 245 (1988).
37. M. J. Crochet, S. Dupont and J. M. Marchal, 'The numerical simulation of the flow of viscoelastic fluids of the differential and integral types: a comparison', *Proc. IX Int. Congr. on Rheology*, Mexico, 1984.
38. R. Keunings, *J. Non-Newtonian Fluid Mech.*, **20,** 209 (1986).
39. G. G. Lipscomb, R. Keunings and M. M. Denn, *J. Non-Newtonian Fluid Mech.*, **24,** 85 (1987).
40. J. M. Marchal and M. J. Crochet, *J. Non-Newtonian Fluid Mech.*, **20,** 187 (1986).
41. J. H. Song and J. Y. Yoo, *J. Non-Newtonian Fluid Mech.*, **24,** 221 (1987).